New Ternary Hafnium Tellurides Hf_8Te_6M (M = Mn, Fe) Containing M-Centered Tetrakaidecahedra

Robert L. Abdon and Timothy Hughbanks*

Department of Chemistry, Texas A&M University, College Station, Texas 77843

Received December 6, 1993®

The synthesis of the new ternary hafnium tellurides Hf_8Te_6M (M = Mn, Fe) is reported. The single-crystal structure of the Mn-containing compound has been determined. Hf_8Te_6Mn crystallizes in the orthorhombic space group *Pmmn* (No. 59) with lattice parameters a = 25.816 (4) Å, b = 3.7614 (6) Å, c = 7.605 (2) Å (Z = 2); the lattice parameters for the Fe analog show a slight shortening of the b axis: a = 25.815 (5) Å, b = 3.7309 (7) Å, c = 7.598 (1) Å. The Hf_8Te_6M structure possesses tricapped trigonal-prismatic Hf clusters centered by M. The trigonal prism dimensions are such that Hf–Hf contacts between triangular faces are long (3.761 Å) and the triangular faces themselves are isosceles (d(Hf–Hf): 2 × 3.160 Å, 3.565 Å). The Te atoms are 4-, 5-, and 6-coordinate with respect to Hf and serve to sheath the metal framework to produce large Te-lined cavities within the structure. Resistivity measurements between 77 and 250 K show Hf_8Te_6Mn to be metallic as predicted by band-structure calculations. The same calculations also indicate that Hf–M bonding is of overriding importance in stabilizing these metal–metal bonded structures. There is no significant Te–Te bonding.

Introduction

Early transition metal chalcogenides have been widely studied because of their unusual structural, physical, and electronic properties. Often these materials show anisotropic electrical conductivity, charge density waves,[1-6] or superconductivity.[7-10] Historically, most attention has focused on sulfides and selenides. The known binary compounds of tellurium suggest that its chemistry may be quite different from that of sulfur and selenium. The MQ_3 (M = Ti, Zr, Hf, Nb, Ta; Q = S, Se)[11-14] compounds are well characterized but have no tellurium counterparts. Tellurium instead forms MTe_4 (M = Nb, Ta) type phases which in turn have no sulfur or selenium analogs.[15,16] The zirconium–tellurium binary system exhibits a rich chemistry in both high and low zirconium oxidation states. In the hafnium–tellurium binary system, the only known compounds are those in which hafnium is fully oxidized. Research currently under way in our laboratory suggests that the chemistry of hafnium and zirconium can be very different in metal-rich, solid-state chalcogenides.

Recent investigations of tantalum- and niobium-rich chalcogenides have produced structurally diverse materials. Layered materials result for Ta_2Se,[17] $Ta_{3.28}Nb_{1.72}S_2$,[18] $Ta_{1.6}Nb_{0.4}S$,[19] Ta_2Te_3,[20,21] $Nb_2Co_2Te_4$,[22] TaM_2Te_2 (M = Co, Ni),[23] and $NbMTe_2$ (M = Fe, Co).[24] These materials contain metal–metal bonded layers which are separated by chalcogen atoms and are held together by weak van der Waals interactions. Other materials in these systems form columnar metal frameworks which are sheathed by chalcogen atoms. Tantalum-centered pentagonal antiprismatic chains $^1_\infty[Ta_5Ta]$ result in Ta_6S,[25,26] Ta_2S,[27] Ta_3S_2,[28] and Ta_6Te_5.[29] Four-fold antiprismatic chains are found in the quasi-one-dimensional Ta_4ZTe_4 and Nb_4ZTe_4 (Z = Al, Si, Cr–Ni) series of compounds.[30]

In this paper we report the synthesis, structural characterization and electrical properties of the new compounds Hf_8Te_6M (M = Mn, Fe). These materials show a close structural resemblance to the condensed cluster tantalum compounds $Ta_9S_6M_2$, $Ta_{11}Se_8M_2$ (M = Fe, Co, Ni),[31-33] and Ta_8Se_8M (M = Ni, Co)[34] all of which contain condensed

* To whom correspondence should be addressed.

® Abstract published in *Advance ACS Abstracts,* March 1, 1994.

(1) Wilson, J. A. *Phys. Rev. B: Condensed Matter* **1979**, *19*, 6456.
(2) Wilson, J. A.; DiSalvo, F. J.; Mahajan, S.; *Adv. Phys.* **1975**, *24*, 117.
(3) Ishihara, Y.; Nakada, I. *Solid State Commun.* **1983**, *45*, 129.
(4) Ishihara, Y.; Nakada, I.; Suzuki, K.; Ichihara, M. *Solid State Commun.* **1984**, *50*, 657.
(5) DiSalvo, F. J.; M., R. T. *Phys. Today* **1979**, *32*, 32.
(6) Rouxel, J. *Crystal Chemistry and Properties of Materials with Quasi-One-Dimensional Structures*; D. Reidel: Dordrecht, Holland, 1986.
(7) Gamble, F. R.; DiSalvo, F. J. *Science* **1970**, *168*, 568.
(8) Ishihara, Y.; Nakada, I. *Solid State Commun.* **1982**, *42*, 579.
(9) Amberger, E.; Polborn, K.; Grimm, P.; Dietrich, M. *Solid State Commun.* **1978**, *26*, 943.
(10) Biberacher, W.; Schwenk, H. *Solid State Commun.* **1980**, *33*, 385.
(11) Bjerkelund, E.; Kjekshus, A. *Acta Chem. Scand.* **1965**, *19*, 701.
(12) Rijnsdorp, J.; Jellinek, F. *J. Solid State Chem.* **1978**, *25*, 325.
(13) Bjerkelund, E.; Kjekshus, A. *Z. Anorg. Allg. Chem.* **1964**, *B328*, 235.
(14) Meerschaut, E.; Guemas, L.; Rouxel, J. *J. Solid State Chem.* **1981**, *36*, 118.
(15) Selte, K.; Kjekshus, A. *Acta Chem. Scand.* **1964**, *18*, 690.
(16) Bjerkelund, E.; Kjekshus, A. *J. Less-Common Met.* **1964**, *7*, 231.
(17) Harbrecht, B. *Angew. Chem., Int. Ed. Engl.* **1989**, *28*, 1660.
(18) Yao, X.; Franzen, H. F. *J. Am. Chem. Soc.* **1991**, *113*, 1426.
(19) Nanjundaswamy, K. S.; Hughbanks, T. *J. Solid State Chem.* **1992**, *98*, 278.
(20) Tremel, W. *Angew. Chem., Int. Ed. Engl.* **1991**, *103*, 900.
(21) Conrad, M.; Harbrecht, B. *J. Alloys Compounds* **1992**, *187*, 181.
(22) Tremel, W. *J. Chem. Soc., Chem. Commun.* **1991**, 1405.
(23) Tremel, W. *Angew. Chem., Int. Ed. Engl.* **1992**, *31*, 217.
(24) Li, J.; Badding, M. E.; DiSalvo, F. J. *Inorg. Chem.* **1992**, *31*, 1050.
(25) Franzen, H. F.; Smeggil, J. G. *Acta Crystallogr. Sect. B* **1970**, *26*, 125.
(26) Harbrecht, B. *J. Less Common Met.* **1988**, *138*, 225.
(27) Franzen, H. F.; Smeggil, J. G. *Acta Crystallogr. Sect. B* **1969**, *25*, 1736.
(28) (a) Kim, S.-J.; Nanjundaswamy, K. S.; Hughbanks, T. *Inorg. Chem.* **1991**, *30*, 159. (b) Wada, H.; Onoda, M. *Mater. Res. Bull.* **1989**, *24*, 191.
(29) Conrad, M.; Harbrecht, B. In *IVth Euro. Conf. on Solid State Chem.*; Gesellschaft, Deutscher Chemiker: Dresden, Germany, 1992; pp 324, cited in ref 32.
(30) Badding, M. E.; DiSalvo, F. J. *Inorg. Chem.* **1990**, *29*, 3952.
(31) Harbrecht, B.; Franzen, H. F. *J. Less Common Met.* **1985**, *113*, 349.
(32) Harbrecht, B. *J. Less-Common Met.* **1986**, *124*, 125.
(33) Harbrecht, B. *J. Less Common Met.* **1988**, *141*, 59.
(34) Conrad, M.; Harbrecht, B. *J. Alloys Compounds* **1993**, *197*, 57.

0897-4756/94/2806-0424$04.50/0

Table 1. Lattice Parameters (Å) of Hf_8Te_6M Phases (Space Group *Pmmn*)[a]

	Hf_8Te_6Mn	Hf_8Te_6Fe
a	25.816(4)	25.815(5)
b	3.7614(6)	3.7309(7)
c	7.605(2)	7.598(1)

[a] Refined from Guinier powder diffraction patterns using Si as an internal standard.

tetrakaidecahedral tantalum clusters centered by a transition element, M.

Experimental Procedures

Syntheses. Hf (99.6%, including 2.9% Zr, Johnson Matthey), Te (99.99%, Johnson Matthey), Mn (99.9%, Aldrich), and Fe (99.99+%, Aldrich) were used as starting materials. Hf_8Te_6Fe was first discovered from the reaction of $HfTe_2$, Hf, and Fe at a molar ratio of Hf:Te:Fe of 4:4:1 in sealed Ta capsules in turn sealed in evacuated silica tubes. The temperature of the reaction vessel was ramped uniformly to 975 °C over 2 days. The reaction was held at this temperature for 12 days before being radiatively quenched to room temperature. Guinier powder films showed a small amount of residual $HfTe_2$ as the only identifiable phase. Attempts to grow single crystals via vapor-phase transport using $TeCl_4$ repeatedly produced only very small needle-shaped crystals. By substitution of Mn for Fe and use of the same reaction conditions, long black needlelike crystals were obtained (typical dimensions: 0.001 × 0.75 × 0.001 mm). The Guinier powder pattern for these needles is nearly identical to that of the iron-containing phase. Microprobe analysis of these crystals gave the approximate composition $Hf_{7.9}Te_{5.7}Mn$. No impurity elements heavier than Na were found. Selection of a crystal suitable for single-crystal X-ray study was difficult as most crystals tended to grow very long and very thin.

Crystals of suitable size for X-ray diffraction experiments are most easily prepared when an excess of Mn is employed. The crystal used in the structure determination was taken from a reaction containing a total of 0.3 g of the elements in the molar ratio Hf:Te:Mn = 6:3:1. After the structure and composition were determined, a powder sample of Hf_8Te_6Mn was obtained in quantitative yield by heating a stoichiometric mixture of the elements at 1000 °C for 10 days. The powder diffraction pattern of this sample matched the pattern calculated from the crystal structure.

X-ray Studies. A black needle-shaped crystal having approximate dimensions of 0.02 × 0.34 × 0.02 mm was mounted in a glass capillary. Preliminary oscillation and Weissenberg photos established an orthorhombic unit cell and gave approximate lattice parameters. All measurements were made on a Siemens R3m/V diffractometer with graphite-monochromated Mo Kα radiation at room temperature. Cell constants and an orientation matrix were obtained from a least-squares refinement using setting angles of eight centered reflections. This cell was refined by centering on 24 reflections in the range $15 < 2\theta < 30$ degrees. The cell parameters (refined from Guinier powder diffraction patterns) for both the Mn- and the Fe-containing compound are given in Table 1. Data were collected by θ–2θ scans for reflections with $2\theta < 50°$. Three check reflections were monitored periodically and showed no significant change during the 2-day data collection process. Two octants of data were collected ($\pm h,+k,+l$) to gain the advantage of averaging. The data were corrected for absorption using the Ψ-scan technique based on three reflections. Systematic absences reduced the possible space groups to $Pmn2_1$ (No. 31) and *Pmmn* (No. 59). After applying the absorption correction, all atoms were located by direct methods in the centrosymmetric space group *Pmmn*.

The structure was refined on F^2 using SHELX 93[35] to residuals of 3.10 and 5.90% for *R* and R_w, respectively. Large thermal ellipsoids directed along the *b* axis for all atoms after anisotropic refinement suggested an additional absorption problem. After correcting for absorption with DIFABS, anisotropic refinement gave generally isotropic thermal ellipsoids, although Hf3 remained somewhat elongated (U_{22}:U_{11} = 3.2, U_{22}:U_{33} = 2.3). The structure was refined to final values for *R* and R_w of 3.12 and 6.28%, respectively. The largest remaining peaks in the final Fourier difference map were 3.862 and −2.267 e⁻/Å³. A summary of crystal and data collection parameters may be found in Table 2; final atomic coordinates are located in Table 3.

(35) Sheldrick, G. M. In Nicolet Analytical X-ray Instruments: Göttingen, Germany, 1988.

Table 2. Crystallographic Data for Hf_8Te_6Mn

chemical formula	Hf_8Te_6Mn
V, Å³	741.5(6)
Z	2
formula weight	2248.503
space group	*Pmmn* (No. 59)
T, °C	23
λ, Å	0.71073
abs coeff (μ) (Mo Kα), mm⁻¹	68.075
crystal dimens, mm	0.02 × 0.34 × 0.02
2θ(max), deg	50
no. of reflns	
measd ($\pm h,k,l$)	1530
unique	783 (R_{int} = 5.24%)
unique obsd ($F_o^2 > 4\sigma(F_o^2)$)	568
no. of variables	50
secondary ext coeff (10^{-4})	2.4(6)
R;[a] R_w[b], % ($I\ 2\sigma(I)$)	3.12; 6.28
R;[a] R_w[b], % (all data)	5.63; 6.94
goodness of fit indicator	1.018
max (min) peaks in final diff map	3.862 (−2.267) e⁻/Å³

[a] $R = \Sigma(|F_o|-|F_c|)/\Sigma|F_o|$. [b] $R_w = [\Sigma w(|F_o|-|F_c|)^2]^{1/2}, w = 4F_o^2/\sigma^2(F_o^2)$.

Table 3. Positional Parameters for Hf_8Te_6Mn

	x	*y*	*z*	*U* (eq)
Hf1	0.6509 (1)	1/4	0.4450 (2)	9 (1)
Hf2	0.5514 (1)	3/4	0.5590 (2)	12 (1)
Hf3	3/4	3/4	0.4230 (2)	10 (1)
Hf4	0.6810 (1)	3/4	0.7659 (2)	10 (1)
Hf5	3/4	1/4	0.0459 (2)	10 (1)
Te1	0.6680 (1)	3/4	0.1507 (2)	6 (1)
Te2	0.5934 (1)	1/4	0.8020 (2)	8 (1)
Te3	0.5480 (1)	1/4	0.2762 (2)	8 (1)
Mn1	3/4	1/4	0.6768 (7)	6 (1)

Results and Discussion

The Hf_8Te_6M structure exhibits a novel transition-metal framework best described as an intergrowth of distorted M-centered tetrakaidecahedral Hf clusters and edge-sharing hafnium telluride chains. The Te atoms serve to sheath the three-dimensional metal framework and produce large cavities within the structure. The structure is shown in Figure 1 projected onto the *a*,*c* plane. In this depiction only the metal–metal bonding framework is shown. The atom labeling scheme for the unit cell is shown in **1**.

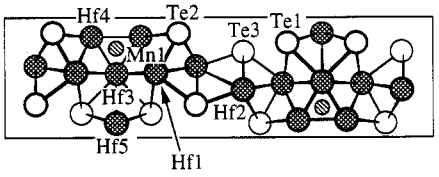

1

The chains of M-centered clusters in the Hf_8Te_6M structure are built up from Hf_3 triangles stacked along the *b* axis to form infinite chains of trigonal prisms. Each of the three square faces of these prisms is capped by another Hf atom. At the center of each trigonal prism sits an M

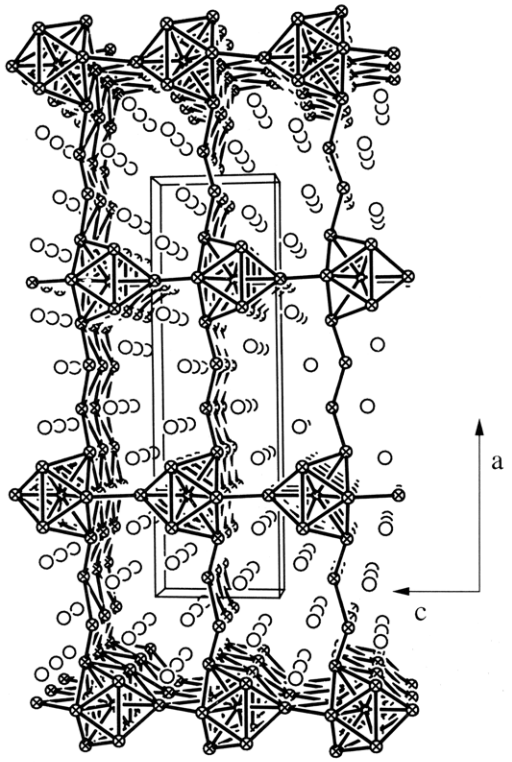

Figure 1. (010) projection of the Hf_8Te_6Mn structure. Hf atoms are shown as the hatched circles, Mn as the small open circles, and Te as the large open circles. Bonds shown indicate the Hf–Hf and Hf–Mn contacts.

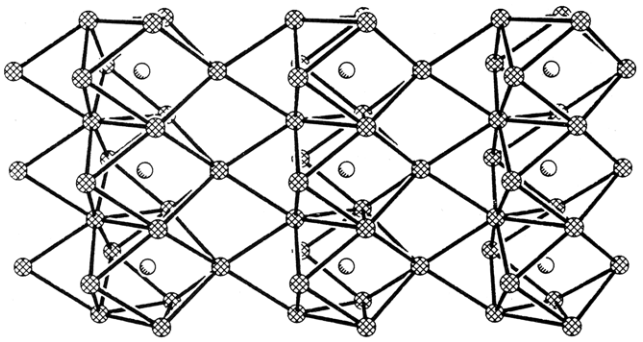

Figure 2. Approximate (100) view of an Hf_6Mn layer showing cluster linkage in the Hf_8Te_6M structure (b axis vertical). Hf atoms are shown as the hatched circles, Mn as the small shaded circles. Only Hf–Hf contacts are depicted as bonds.

atom. The columns are linked by bonds between a hafnium atom of each inner trigonal prism and a capping hafnium of a neighboring chain's cluster, yielding a two-dimensional layer that propagates in the *b*,*c* plane. The unit cell contains two such layers running in opposite directions and stacked along the *a* axis. The Hf–Mn network from one such layer is shown in Figure 2. The portion of the structure connecting these slabs is closely related to a portion of the Hf_3Te_4 structure (Nb_3Te_4-type).[36] In the Hf_3Te_4 structure each Hf atom is surrounded by a distorted tellurium octahedron. Two of the edges of these octahedra are bridged by Hf atoms from neighboring octahedra to produce zigzag Hf chains. In Hf_8Te_6Mn, the Hf atoms between the slabs are five-coordinate with respect to tellurium and in place of a sixth Te atom that would be an apical ligand in an octahedron there are two Hf atoms. This produces a distorted 4^4 Hf net which serves to stitch

(36) Wang, C. C.; Abdon, R. L.; Hughbanks, T., to be submitted.

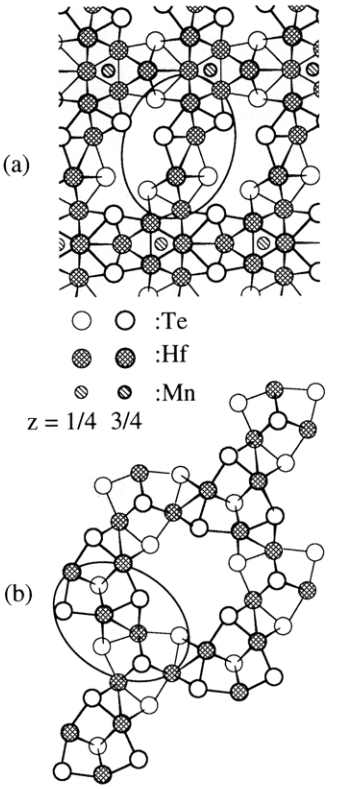

Figure 3. Projections of the (a) Hf_8Te_6M (010) and (b) Hf_3Te_4 (001) structures. The hafnium telluride zigzag chains are circled in each structure.

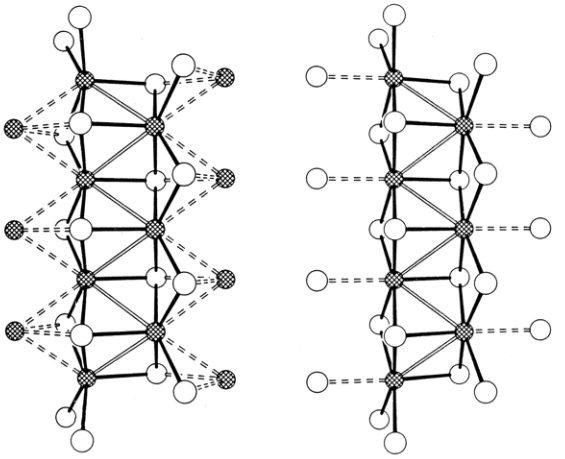

Figure 4. Enlarged view of the zigzag chain environments in the Hf_8Te_6M (left) and Hf_3Te_4 (right) structures. Hf are the cross-hatched circles, and Te are the open circles.

together the layers of condensed clusters (Figures 3 and 4).

The Hf_6Mn trigonal prisms which form the inner cluster core are shaped such that the short Hf–Hf contacts are all in the triangular faces. These faces are distorted in an isosceles fashion forming one long (3.565 Å) and two short (3.160 Å) Hf–Hf contacts. The triangles are separated from each other by the *b*-axis dimension, 3.761 Å. This is much longer than the corresponding Ta–Ta distances in the structurally related $Ta_9S_6M_2$, $Ta_{11}Se_8M_2$, and Ta_8Se_8M compounds. Distances within the M clusters of Hf_8Te_6Mn and Ta_8Se_8Ni are compared in **2**, the most significant difference between the clusters is the distortion of the triangular faces of Hf_8Te_6Mn. The shortest distances between triangular faces occurs in the related

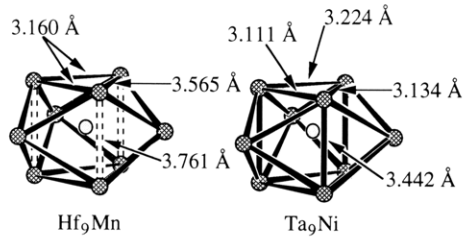

a b

2

sulfide, $Ta_9S_6Fe_2$ (3.297 Å). This distance in the related selenides is somewhat longer (~3.45 Å). In Hf_8Te_6Mn, short Hf–Hf distances between triangular faces are structurally excluded by the packing requirements of the Te atoms, and as we discuss below, the lower metal-based electron concentration in the Hf compounds is consistent with this feature.

Detailed investigation of the structures of the $Ta_9S_6M_2$ materials shows a doubling of the chain axis in the Fe and Co compounds[33] associated with alternating long and short M–M contacts. In $Ta_9S_6Ni_2$ no such pairing of the Ni atoms occurs. Although the presence of the same M-centered tetrakaidecahedral building blocks suggests that such a distortion might also occur in Hf_8Te_6Mn, strongly overexposed oscillation photographs show that no axis doubling occurs. The absence of pathological thermal parameters would also tend to rule out any short-range distortion associated with a pairing distortion. A collection of important distances for Hf_8Te_6Mn are recorded in Table 4.

Investigations into the thermal stability of Hf_8Te_6M compounds show their existence over a wide temperature range. High-temperature, arc-melting reactions have produced Hf_8Te_6Mn as well as a small fraction of a familiar but, as yet, unidentified binary phase. Although synthetic conditions require temperatures in excess of 950 °C, once formed Hf_8Te_6Mn and Hf_8Te_6Fe are stable when annealed at 800 °C.

The importance of Te–Te bonding in transition-metal ditellurides is well documented.[37] The ability of later transition metals in higher formal oxidation states to effectively oxidize Te results in Te–Te bond formation. In $IrTe_2$ for example, the +4 oxidation state for Ir is avoided by formation of Te–Te bonds. Overlap of the Ir 5d bands and the Te 5p bands results in a flow of electrons from the latter to the former, concomitant with Te–Te bond formation. In general, a balance exists between cation–anion redox competition and the avoidance of highly oxidized transition metals. Both factors result in oxidation of Te, producing polymeric Te–Te bonded network structures. The same effect has been found in the ternary $MM'Te_4$ compounds (M = Nb, Ta; M′ = Ru, Os, Rh, Ir)[38] where the structure is stabilized through Te–Te bond formation while the transition metals are reduced despite the weakened metal–metal bonding that results. In metal-rich compounds of the early transition metals, fully reduced Te can be expected. In these materials, early transition metals in low oxidation states have d bands which lie above the Te 5p bands and the latter bands remain entirely filled. No "internal oxidation–reduction" occurs. In Hf_8Te_6Mn, the shortest Te–Te distance is determined by the *b*-axis dimension, 3.761 Å. While this is shorter than the van der Waals distance of 4.0 Å, this separation is a balance between the drive toward shorter Hf–Hf bonds and the avoidance of nonbonded Te–Te repulsions.

Table 4. Important Interatomic Distances (Å) for Hf_8Te_6Mn[a,b]

Hf^i–Hf^i		6-coord Te	
Hf3–Hf4	3.1596 (2)	Te1–Hf1 (2×)	2.957 (2)
Hf4–Hf4a	3.565 (3)	Te1–Hf3 (1×)	2.961 (2)
Hf^i–Hf^a		Te1–Hf4 (1×)	2.945 (2)
Hf3–Hf1	3.181 (1)	Te1–Hf5 (2×)	2.942 (2)
Hf4–Hf1	3.178 (2)	5-coord Te	
Hf3–Hf5	3.429 (2)	Te2–Hf2 (2×)	2.851 (2)
Hf4–Hf5	3.353 (2)	Te2–Hf4 (2×)	2.954 (2)
Hf^a–Hf^z		Te2–Hf1 (1×)	3.094 (2)
Hf1–Hf2	3.299 (2)	4-coord Te	
Hf^z–Hf^z		Te3–Hf1 (2×)	2.957 (2)
Hf2–Hf2a	3.373 (2)	Te3–Hf2 (2×)	2.858 (2)
Mn–Hf^i			
Mn1–Hf3	2.695 (4)		
Mn1–Hf4	2.678 (2)		
Mn–Hf^a			
Mn1–Hf1	3.108 (4)		
Mn1–Hf5	2.807 (6)		

[a] Hf^i:Hf atom of inner trigonal prism. Hf^a:Hf atom capping the trigonal prism. Hf^z:Hf atom of zigzag chain. Atom labels are consistent with illustration 1. [b] Distances were calculated using cell parameters reported in Table 1.

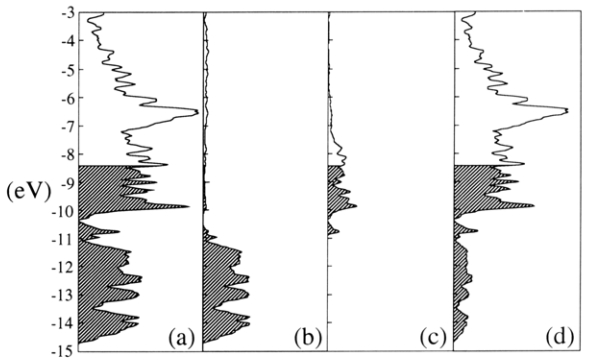

Figure 5. (a) Total density of states (DOS) diagram for Hf_8Te_6Mn. The energy range includes the Te 5p bands and the transition metal d and s bands. (b) Tellurium contribution to the DOS. (c) Mn contribution to the DOS. (d) Hf contribution to the DOS. Filled levels are shaded.

The band structure of Hf_8Te_6Mn was calculated using the extended Hückel method, parameters for which are given in the Appendix. The total density of states (DOS) diagram (Figure 5a) shows that the compound should be a metallic conductor, in accordance with structural intuition. The projected DOS in (b) shows that the levels between −15 and −10.5 eV are primarily Te based while the projections in (c) and (d) show that the higher energy levels have mainly Hf and Mn d and s character. This latter panel shows that significant Hf–Te covalency induces mixing of Hf-based orbitals into the Te-based manifold. The projected DOS in panel (c) indicates that the levels with Mn character are confined to the range between −10.8 and −6.0 eV.

It is interesting to note the segregation of bonding interactions in this material. The manganese contributions are almost entirely excluded from the Te-based levels, despite the small energy separation of the tellurium 5p and manganese 3d and 4s orbital energies. The segregation of interactions into primarily Hf–Te and Hf–Mn regimes

(37) Canadell, E.; Jobic, S.; Brec, R.; Rouxel, J.; Whangbo, M. *J. Solid State Chem.* **1992**, *99*, 189.
(38) Mar, A.; Jobic, S.; Ibers, J. A. *J. Am. Chem. Soc.* **1992**, *114*, 8693.

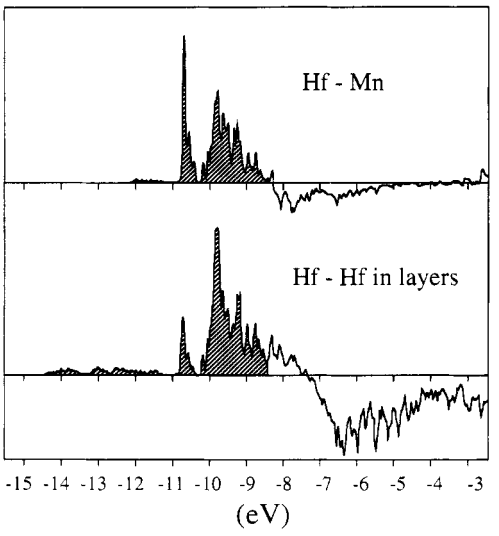

Figure 6. Crystal orbital overlap population (COOP) curves showing averaged Hf–Mn interactions and Hf–Hf interactions within one layer. Levels above the energy axis are bonding while those below are antibonding. Filled levels are shaded. Note optimization of the Hf–Mn interactions in the Hf_8Te_6M structure.

arises directly from the spatial separation of the elements within the structure—there are no Mn–Te bonds.

Crystal orbital overlap populations (COOPs) were also calculated for the metal–metal bonded framework of Hf_8Te_6Mn (see Figure 6).[39] The triangular faces of the Hf trigonal prisms are held together by bonding interactions with the capping Hf atoms as well as the centering M atom. The triangles are separated by the *b*-axis length of (3.7614 Å, Mn; 3.7309 Å, Fe) which is too long for substantial interaction. This is consistent with the calculated overlap populations. Within the metal framework the overlap populations are largest for Hf–Mn interactions (average 0.341) followed by the overlap between the capping Hf atoms and the Hf atoms of the inner triangles (average 0.310). The overlap population between Hf atoms of opposite triangular faces is quite small (0.086). This is also the case for Mn–Mn overlap (−0.008). Figure 6 shows the COOP curve for averaged Hf–Hf interactions within one layer and also averaged Hf–Mn interactions. There are still some Hf–Hf bonding orbitals unoccupied in these materials, as evidenced by the appearance of positive Hf–Hf contributions above the Fermi level. On the other hand, Hf–M bonding is optimal for these materials' electron concentrations, more or fewer electrons would weaken Hf–M bonds. We expect to exploit the stabilization conferred by strong Hf–M bonding in future synthetic exploration of Hf–Te–M systems.

(39) Hughbanks, T.; Hoffmann, R. *J. Am. Chem. Soc.* **1983**, *105*, 3528.

Table 5. Parameters for EH Calculations

	orbital	H_{ii}, eV	$\zeta 1^b$	$\zeta 2^b$	$c1^a$	$c2^a$
Hf	5d	−8.14	4.36	1.709	0.6967	0.5322
	6s	−8.12	2.21			
	6p	−4.50	2.17			
Mn	3d	−8.70	5.32	1.900	0.5047	0.6805
	4s	−7.50	1.80			
	4p	−3.80	1.80			
Te	5s	−21.20	2.51			
	5p	−12.00	2.16			

[a] Coefficients used in double-ζ expansion. [b] Slater-type orbital exponents.

Preliminary resistivity measurements between 77 and 250 K confirm metallic behavior (positive temperature coefficient). Above 250 K the behavior is not simple and the residual resistivity extrapolated to $T = 0$ K appears to be quite high. The unusual electronic and magnetic properties of these materials are currently under further investigation.

Acknowledgment. This research was generously supported by the National Science Foundation through Grant DMR-9215890 and by the Robert A. Welch Foundation through Grant A-1132. We thank Yunchao Tian for assistance in performing band-structure calculations, Kyungsoo Ahn for assistance with the resistivity measurements, and Joseph Reibenspies for generous help in X-ray data collection and structure solution. The $R3m/v$ single-crystal X-ray diffractometer and crystallographic computing system were purchased from funds provided by the National Science Foundation (CHE-8513273).

Appendix

The extended Hückel method[40,41] was used for all band structure calculations; parameters appear in Table 5. Valence-state ionization energies (H_{ii}'s) for Hf were previously obtained from a charge-iterative calculation on Hf_2S.[42] Other parameters have been cited previously.[43,44] Band structure calculations were carried out using a 48K point mesh for the 3-D orthorhombic cell. DOS curves were smoothed with Gaussian functions with a half-width of 0.025 eV.

Supplementary Material Available: Table of anisotropic displacement parameters (1 page); table of observed and calculated structure factor data for Hf_8Te_6Mn (5 pages). Ordering information is given on any current masthead page.

(40) Hoffmann, R. *J. Chem. Phys.* **1963**, *39*, 1397.
(41) Whangbo, M.; Hoffmann, R. *J. Am. Chem. Soc.* **1978**, *100*, 6093.
(42) Hughbanks, T., unpublished research.
(43) Basch, H.; Gray, H. B. *Theor. Chim. Acta* **1966**, *4*, 367.
(44) Saillard, J.-Y.; Hoffmann, R. *J. Am. Chem. Soc.* **1984**, *106*, 2006.